Supplementary Information

For Journal of Materials Chemistry A

Perovskite-TiO$_2$@BiVO$_4$ Photoelectrochemical Cells for Unbiased Solar Water Splitting

Xiaofan Zhang[a], Bingyan Zhang[a], Kun Cao[a], Jérémie Brillet[b], Jianyou Chen[a],

Mingkui Wang[a] and Yan Shen[a]*

[a] Wuhan National Laboratory for Optoelectronics, Huazhong University of Science and Technology, Luoyu Road 1037, Wuhan, 430074, P. R. China. *Corresponding author. E-mail: ciac.sheny@mail.hust.edu.cn

[b] Shanghai Institute of Ceramics, Chinese Academy of Sciences, 1295 Dingxi Road, Shanghai 200050 P. R. China

The power conversion efficiency (η) of the perovskite solar cell is calculated according to the following formula:

$$\eta\,(\%) = P_{out}/P_{in} = (FF \times J_{sc} \times V_{oc})/P_{in} \qquad (S1)$$

where P_{in} (100 mW cm^{-2} herein) and P_{out} are the incident light intensity and output power of the solar cell device, FF is the fill factor, and J_{sc} and V_{oc} stand for the short-circuit current density and open-circuit voltage of the solar cell, respectively.
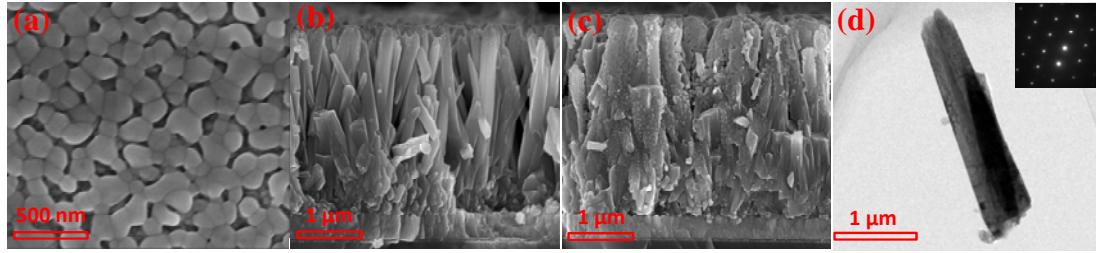
The overall solar-to-hydrogen (STH) efficiency of the PV/PEC cell is calculated with the following equation:

$$STH = \frac{1.23 \times J_{PEC\,cell} \times \eta_F}{P_{in}} \times 100\% \qquad (S2)$$

where $J_{PEC\,cell}$ is the maximum photocurrent given by the photoelectrochemical cell, η_F is the Faradic efficiency for the H$_2$ evolution that can be calculated with the following equation:

$$\eta_F = \frac{2 \times n_{H_2} \times 96485}{Q_c} \times 100\% \qquad (S3)$$

Fig. S1 The SEM images of $BiVO_4$ (a), and the cross-section images of TiO_2 NRs (b) and $TiO_2@BiVO_4$ heterojunction film (c). (d) TEM image of TiO_2 NRs, the inset is the selected area electron diffraction (SAED) pattern.

The elemental compositions were collected by X-ray photoelectron spectroscopy (XPS, AXIS-ULTRA DLD-600 W, Shimdzu) under ultrahigh vacuum ($<10^{-8}$ Torr) and using a monochromatic Al Kα X-ray source operating at 150 W. The survey and high-resolution spectra were collected at fixed analyzer pass energies of 160 and 20 eV, respectively. The binding energy shifts were corrected using the C1s level at 284.8 eV as an internal standard, to compensate for the surface-charging effect during data analysis.
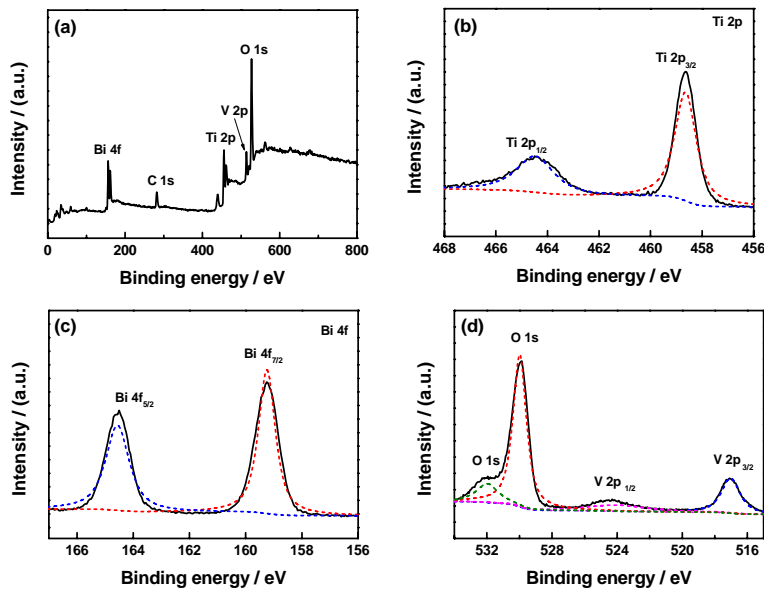
Fig. S2 XPS spectra of the $TiO_2@BiVO_4$ composite film.

Fig. S3 exhibits both the characteristic Raman modes of the rutile TiO_2 and the monoclinic $BiVO_4$. The mode at 146 cm^{-1} (B_{1g}), 443 cm^{-1} (E_g), 609 cm^{-1} (A_{1g}). and 243 cm^{-1} (E_g) is the characteristic peak of the rutile TiO_2. The strongest peak at 826 cm^{-1} and the shoulder peak at 717 cm^{-1} are from the anti-symmetric and symmetric stretching modes of the VO_4 tetrahedral, respectively. The peaks at 325 cm^{-1} and 366 cm^{-1} belong to the bending modes of the VO_4 tetrahedral. The remaining Raman peaks at 129 cm^{-1} and 211 cm^{-1} are attributed to the vibration of the crystal lattice.
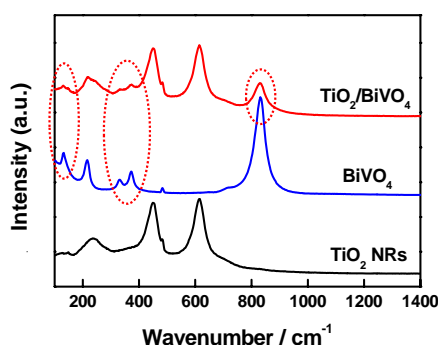
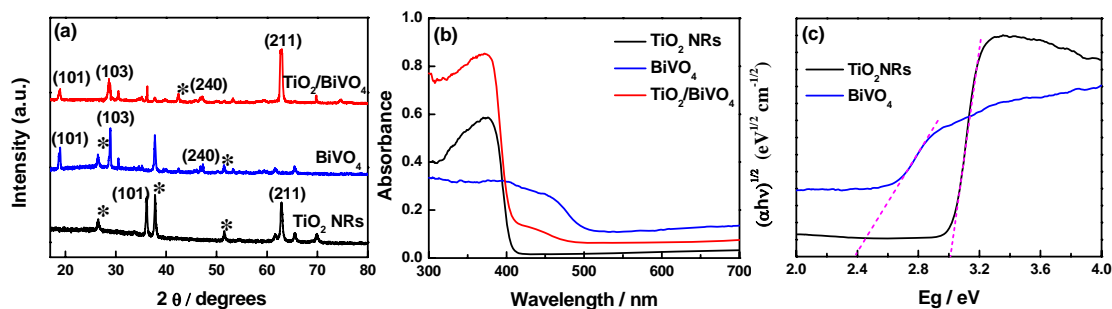**Fig. S3** Raman spectrum for TiO_2 NRs, $BiVO_4$ NPs and $TiO_2@BiVO_4$ composite films.

The phase purity and crystal structure of the obtained samples were examined by X-ray diffraction (XRD). The XRD patterns for the TiO_2 NRs and $BiVO_4$ NPs are displayed in Fig. S4a, corresponding to a pure tetragonal rutile TiO_2 and monoclinic $BiVO_4$ phase, respectively. After deposition of the $BiVO_4$, only rutile TiO_2 and monoclinic $BiVO_4$ phase are detected in the XRD pattern of $TiO_2@BiVO_4$ composite film, suggesting that the phase and composition of the TiO_2 is unchanged after deposition the $BiVO_4$ NPs. Fig. S4b compares the UV-visible absorption of the samples. The optical band gap can be estimated by dropping a line from the maximum slope of the Tauc plot ($\sqrt{\alpha h\nu}$ vs $h\nu$) to the axis (Fig. S4c).[3] Therefore, the band tail was estimated to be 2.4 and 3.0 eV for the $BiVO_4$ NPs and TiO_2 NRs, respectively. Compared to the TiO_2 NRs, the $TiO_2@BiVO_4$ photoanode exhibits an increase in light absorption intensity in the range from 300 to 500 nm. The broad absorption band

from 400 to 500 nm could be attributed to the light absorption of $BiVO_4$, which remarkably enhances the TiO_2 light absorption ability.

Fig. S4 (a) XRD patterns of the TiO_2 NRs, $BiVO_4$ NPs and $TiO_2@BiVO_4$ composite film. Asterisks ($*$) is corresponding to diffraction peaks arising from the FTO substrate. (b) UV-vis absorption spectrum for all prepared samples. (c) Tauc plots of TiO_2 NRs and $BiVO_4$ NPs for the band gap calculation.

Table S1. Comparison of various TiO_2-$BiVO_4$ photoanodes for PEC water splitting.

Electrolyte solution	Photocurrent density at 1.23 V *vs.* RHE (mA cm^{-2})	Reference
1 M NaOH	0.2 (visible light)	1
0.1 M K_3PO_4 (pH 8.0)	0.15 (full solar spectrum)	2
0.1 M PBS (pH 7.0)	1.3 (full solar spectrum) 0.81 (λ>420 nm)[a]	This work

[a] This photocurrent density is calculated by integrating the measured IPCE (Figure 3b) over standard AM 1.5 G spectrum within the region λ>420 nm.

1
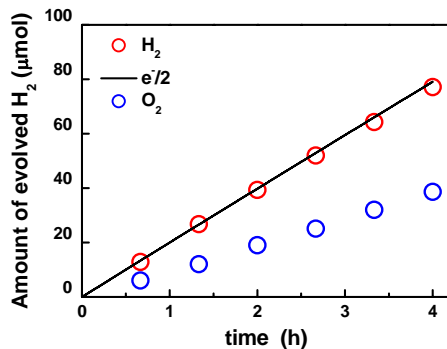
Fig. S5 PEC water splitting of the $TiO_2@BiVO_4$ photoanode at 1.23 V vs. RHE (the theory potential of water decomposition) in three-electrode system under irradiation. Black line corresponds to the integration over time of the net photocurrent divided by 2. Blue and red circles correspond to the evolved O_2 and H_2 gas measured by gas chromatography during the experiment, respectively.

The absorbed photo-to-current efficiency (APCE) was obtained by dividing the IPCE by light harvesting efficiency (LHE) at each wavelength using the formula with APCE=IPCE/LHE, and the LHE plots of the samples are shown in Fig. 4a. In order to explain the fact that more photogenerated holes with my structure can be collected than the mesoporous structure, the normalized APCE was obtained (Fig. S6).
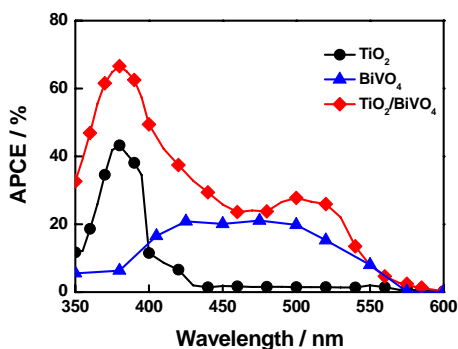
Fig. S6 APCE plots of the TiO_2 NRs, $BiVO_4$ and $TiO_2@BiVO_4$ photoanodes.
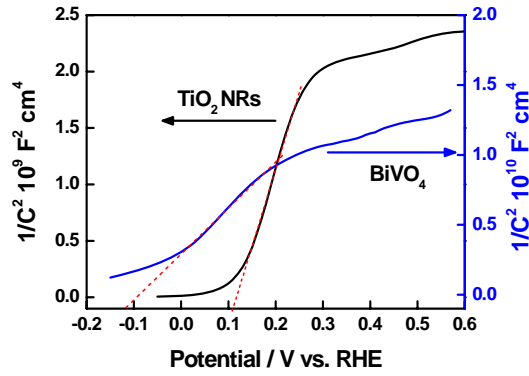
1

2 **Fig. S7** Mott-Schottky plots of the TiO_2 NRs (black line) and $BiVO_4$ NPs (blue line).

3

4   The applied bias photon-to-current efficiency (ABPE) was calculated from the J-V

5 curves obtained from a two-electrode system where V_{bias} is the applied bias between

6 WE and CE assuming 100% Faradaic efficiency using the following equation, [4]

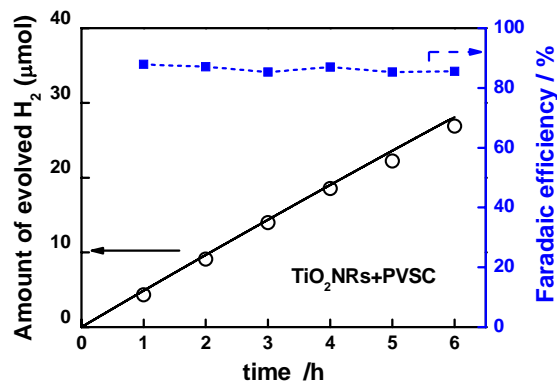7 $$ABPE = \frac{J_p \times (1.23 - |V_{bias}|)}{P_{in}} \times 100\% \qquad (S4)$$

8 where J_p is the photocurrent density (mA cm^{-2}), V_{bias} is the applied bias between the

9 working electrode and counter electrode (V), and P_{in} is the inciden illumination power

10 density (AM 1.5G, 100 mW/cm^2).
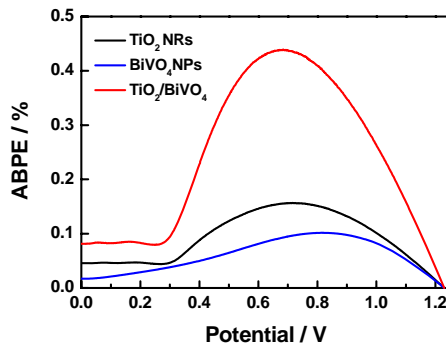
11

12 **Fig. S8** ABPE plots of all photoanodes obtained using a two-electrode system.

13

Fig. S9 The Faradaic efficiency and quantity of detected hydrogen derived from the TiO$_2$ NRs+PVSC device under irradiation. Black line corresponds to the integration of the net photocurrent divided by 2. Black circle corresponds to the H$_2$ gas measured by gas chromatography during the experiment.

Electrochemical impedance spectroscopy measurement was further performed at open circuit potential under AM 1.5G illumination. Fig. S8 presents the typical Nyquist plots for various photoanodes. An equivalent circuit model (the inset of Fig. S8) was employed to analyze the EIS data, in which R$_s$ is the resistance of the electrolyte, C$_p$ is the capacitance phase element, and R$_{ct}$ represents the charge-transfer resistance at the photoanode/electrolyte interface where the water oxidation reaction occurred.[5] Normally, a decrease of the charge transfer resistance indicates a fast interfacial charge transfer process. Here, the TiO$_2$@BiVO$_4$ heterojunction photoanode exhibits the smallest charge transfer resistance among the three samples, which indicates a more effective separation of photogenerated carriers and faster interfacial charge transfer occurring in the TiO$_2$@BiVO$_4$ photoanode. This result is consistent with the PEC measurements that the TiO$_2$@BiVO$_4$ sample shows the best PEC water oxidation performance.
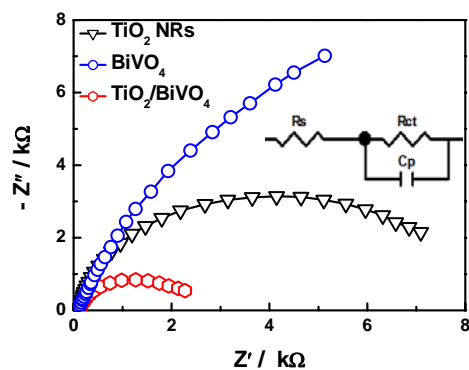
Fig. S10 Nyquist EIS plots for all photoanodes at open circuit potential recorded under light illumination. The inset is the equivalent circuit model used for fitting the experimental data (The solid lines are the fitting results, the circles are the experimental results).

Reference

1. M. Xie, X. Fu, L. Jing, P. Luan, Y. Feng, H. Fu, *Adv. Energy Mater*. 2014, **4**, 1300995.

2. S. Kimura, S. Moniz, A. Handoko, J. Tang, *J. Mater. Chem. A,* 2014, **2**, 3948-3953.

3. X. Zhang, B. Zhang, D. Huang, H. Yuan, M. Wang and Y. Shen, Carbon, 2014, **80**, 591-598.

4. T. Kim, K. Choi, *Science* 2014, **343**, 990-994.

5. M. Wang, P. Chen, R. Baker, S. Zakeeruddin and M. Grätzel, *ChemPhysChem,* 2009, **10**, 290-299.